Journal of Power Sources 214 (2012) 7–14

Contents lists available at SciVerse ScienceDirect

Journal of Power Sources

journal homepage: www.elsevier.com/locate/jpowsour

$(Y_{0.5}In_{0.5})Ba(Co,Zn)_4O_7$ cathodes with superior high-temperature phase stability for solid oxide fuel cells

Y.N. Kim [a], J.H. Kim [b], A. Huq [b], M.P. Paranthaman [c], A. Manthiram [a,*]

[a] Electrochemical Energy Laboratory & Materials Science and Engineering Program, University of Texas at Austin, Austin, TX 78712, USA
[b] Neutron Scattering Science Division, Oak Ridge National Laboratory, Oak Ridge, TN 37831, USA
[c] Chemical Sciences Division, Oak Ridge National Laboratory, Oak Ridge, TN 37831, USA

A R T I C L E I N F O

Article history:
Received 12 February 2012
Received in revised form
25 March 2012
Accepted 26 March 2012
Available online 22 April 2012

Keywords:
Solid oxide fuel cells
Cathodes
Thermal expansion coefficient
Phase stability

A B S T R A C T

$(Y_{0.5}In_{0.5})BaCo_{4-x}Zn_xO_7$ ($1.0 \le x \le 2.0$) oxides crystallizing in a trigonal *P*31*c* structure have been explored as alternative cathode materials for solid oxide fuel cells (SOFC). At a given Zn content, the $(Y_{0.5}In_{0.5})BaCo_{4-x}Zn_xO_7$ compositions exhibit superior phase stability compared to $YBaCo_{4-x}Zn_xO_7$ and $InBaCo_{4-x}Zn_xO_7$ at the operating temperatures of SOFC (600–800 °C). In the $(Y_{0.5}In_{0.5})Ba(Co_{4-x}Zn_x)O_7$ system, the $x = 1$ sample offers a combination of good electrochemical performance, low thermal expansion coefficient (TEC), and enhanced chemical stability against $Ce_{0.8}Gd_{0.2}O_{1.9}$ (GDC) electrolyte while demonstrating good phase stability at 600–800 °C for 100 h. Optimum cathode performance could be obtained by employing $(Y_{0.5}In_{0.5})BaCo_3ZnO_7$ + GDC (50:50 wt.%) composite cathodes attached at 850 °C for 3 h as evidenced by ac-impedance spectroscopy, and the fuel cell performance of this composite cathode was evaluated using anode-supported single cells. With a combination of excellent high-temperature phase stability, low TEC, and good electrochemical performances, the trigonal $(Y_{0.5}In_{0.5})BaCo_3ZnO_7$ composition is an attractive cathode candidate for intermediate temperature SOFC.

1. Introduction

Mixed oxide-ion and electronic conducting (MIEC) oxides with perovskite and perovskite-related structures have been studied intensively in high-temperature devices such as solid oxide fuel cells (SOFC), sensors, and oxygen permeation membranes. In particular, cobalt-containing oxides have drawn much attention as cathodes in SOFC due to their high fuel cell performance [1–14]. However, their high thermal expansion coefficient (TEC) values attributed to the low-spin to high-spin transition of octahedral-site Co^{3+} ions and the accompanying increase in ionic radius has impeded their practical application in SOFC [4,15–17].

Recently, $RBaCo_{4-x}Zn_xO_{7+\delta}$ (R = Y, Ca, In, Tb, and Eu) oxides have attracted attention as alternative cathode materials for SOFC [18–22]. The $RBaCo_{4-x}Zn_xO_{7+\delta}$ oxides have been reported to crystallize in a trigonal symmetry with the space group *P*31*c* [23] which consists of alternating triangular and Kagomé planes with two different corner-shared $(Co_{4-x}Zn_x)O_4$ tetrahedra layers along the *c*-axis [23,24]. Unlike the Co^{3+} ions in the CoO_6 octahedra in the perovskite lattice, the high-spin state $Co^{2+/3+}$ ions in the $(Co_{4-x}Zn_x)O_4$ tetrahedra does not experience spin-state transitions at the operating temperature of SOFC [18,25]. In addition, the $RBaCo_{4-x}Zn_xO_{7+\delta}$ oxides exhibit relatively a small amount of oxygen-loss on heating as evidenced by the TGA data [18,20]. These properties contribute to the low TEC of the $RBaCo_{4-x}Zn_xO_{7+\delta}$ oxides that is compatible with those of the standard SOFC electrolytes [18,22]. Among the various compositions investigated, the $YBaCo_3ZnO_7$ + GDC composite (50:50 wt.%) has been found to exhibit performance in SOFC superior to that of the perovskite $La_{0.6}Sr_{0.4}Co_{0.2}Fe_{0.8}O_3$ (LSCF) cathode [18,21].

The Zn-free $YBaCo_4O_7$ suffers from phase decomposition into Y_2O_3, $BaCoO_{3-\delta}$, and Co_3O_4 at elevated temperatures of 700–800 °C [18]. Considering the presence of the Co^{3+} ions in octahedral sites in both $BaCoO_{3-\delta}$ and Co_3O_4, the decomposition of $YBaCo_4O_7$ may be related to the tendency of cobalt ions to adopt octahedral coordination although the exact mechanism is not clearly established yet. However, the high temperature phase stability could be greatly improved by a partial substitution of Zn for Co since Zn has a strong preference for tetrahedral coordination and could suppress the tendency of cobalt ions to transition from tetrahedral to octahedral coordination [18,26]. The phase stability of $YBaCo_{4-x}Zn_xO_7$ improves with increasing amount of Zn, but higher Zn contents leads to a decrease in electrical conductivity due to the completely filled 3d orbitals and a consequent degradation in electrochemical

* Corresponding author. Tel.: +1 512 471 1791; fax: +1 512 471 7681.
E-mail address: rmanth@mail.utexas.edu (A. Manthiram).

0378-7753/$ – see front matter © 2012 Elsevier B.V. All rights reserved.
doi:10.1016/j.jpowsour.2012.03.050

performance in SOFC. Therefore, it is critical to develop optimum compositions that can offer a combination good high-temperature phase stability and electrochemical performance in order for this class of materials with an important advantage of low TEC to become competitive as cathodes for SOFC.

The high temperature phase stability is also influenced by the nature of the R^{n+} ions in $RBaCo_{4-x}Zn_xO_{7+\delta}$ although it is not as dominant as the substitution of Zn. In other words, at a given Zn content, the phase stability differs depending on the R^{n+} ions. For example, the $YBaCo_3ZnO_7$ composition was found to be stable after heating at 800 °C for 120 h while it decomposed slightly at 600 and 700 °C for 120 h [19]. In contrast, $InBaCo_3ZnO_7$ was stable after heating at 600 °C for 100 h, but showed partial decomposition at 700 and 800 °C on heating for 100 h [20]. Further increase in Zn content was necessary to enhance the phase stability of $InBaCo_{4-x}Zn_xO_7$, which led to a degradation in electrochemical performances. Since the R = Y and R = In samples in $RBaCo_{4-x}Zn_xO_7$ differ in the temperature range at which they exhibit instability as pointed out above, it will be interesting to see whether the system can be made stable through the entire SOFC operating temperature of 600–800 °C with R = $Y_{0.5}In_{0.5}$. Although our earlier preliminary results indicated a slight phase decomposition at elevated temperatures with $Y_{0.5}In_{0.5}BaCo_3ZnO_7$ [18], we found that a small variation in chemical compositions and Y:In ratio influence the phase stability. Accordingly, we present here a systematic and careful investigation of the $Y_{0.5}In_{0.5}BaCo_{4-x}Zn_xO_7$ system. At a few specific Zn contents (x = 1, 1.5, and 2.0) in the $RBaCo_{4-x}Zn_xO_7$ system, the influences of the mixed R = $Y_{0.5}In_{0.5}$ on the crystal chemistry, phase stability, thermal and electrochemical properties, and fuel cell performances of the $Y_{0.5}In_{0.5}BaCo_{4-x}Zn_xO_7$ cathodes are presented.

2. Experimental

The $(Y_{0.5}In_{0.5})BaCo_{4-x}Zn_xO_7$ samples were prepared by conventional solid-state reaction methods. Required amounts of Y_2O_3 (Alfa Aesar, 99.9%), In_2O_3 (Alfa Aesar, 99.9%), $BaCO_3$ (Alfa Aesar, 99.8%), Co_3O_4 (Alfa Aesar, 99.7%), and ZnO (Alfa Aesar, 99.7%) were thoroughly mixed in a mortar and pestle and calcined at 900 °C for 12 h in air. The calcined powders were then ground, pressed into pellets, and sintered at 1150 °C for 12 h in air. The products thus obtained were characterized by X-ray diffraction (XRD), and the XRD data were refined with the Rietveld method with the GSAS program [27]. In addition, the high temperature XRD of the x = 1.0 sample was measured with increasing temperature after dwelling for 0.5 h at each temperature before recording. The room-temperature oxygen content values were determined by iodometric titration [28]. The $(Y_{0.5}In_{0.5})BaCo_{4-x}Zn_xO_7$ + GDC (Fuel Cell Materials, Micro grade) composite cathodes (50:50 wt.%) were prepared by ball-milling appropriate amounts of $(Y_{0.5}In_{0.5})BaCo_{4-x}Zn_xO_7$ and GDC in ethanol for 3 days.

The phase stabilities of the $(Y_{0.5}In_{0.5})BaCo_{4-x}Zn_xO_7$ powders were assessed by a long-term phase stability measurement, which involves heating the sample powder in platinum crucible at 600, 700, and 800 °C for 100 h to provide enough time for the phase decomposition to occur. The resulting powders were characterized by XRD. The high temperature chemical stability of the $(Y_{0.5}In_{0.5})BaCo_{4-x}Zn_xO_7$ cathode powders in contact with the GDC electrolyte was measured by mixing the cathode and GDC powders in a 1:1 weight ratio, followed by calcining at 800 and 1000 °C for 3 h in air.

The electrical conductivity of the $(Y_{0.5}In_{0.5})BaCo_{4-x}Zn_xO_7$ specimens was measured with a four-probe dc method using a Van der Pauw configuration in the temperature range of 40–900 °C [29,30]. Thermogravimetric analysis (TGA) was performed with a Netzsch (STA 449 F3) thermal analysis system. The TGA experiments were carried out in air for two consecutive heating/cooling cycles at a rate of 3 °C min^{-1} from 80 to 900 °C. After the first heating cycle, the sample was allowed to dwell at 900 °C for 15 h to stabilize before recording the first cooling curve. Thermal expansion data were collected in air with a dilatometer (Linseis L75H) during three consecutive heating/cooling cycles at a rate of 3 °C min^{-1} between 20 and 900 °C with an intermediate dwelling at 900 °C for 1 h.

The polarization resistance (R_p) of the $(Y_{0.5}In_{0.5})BaCo_{4-x}Zn_xO_7$ + GDC composite cathode in contact with GDC pellets was measured with symmetrical cells in the temperature range of 400–750 °C by

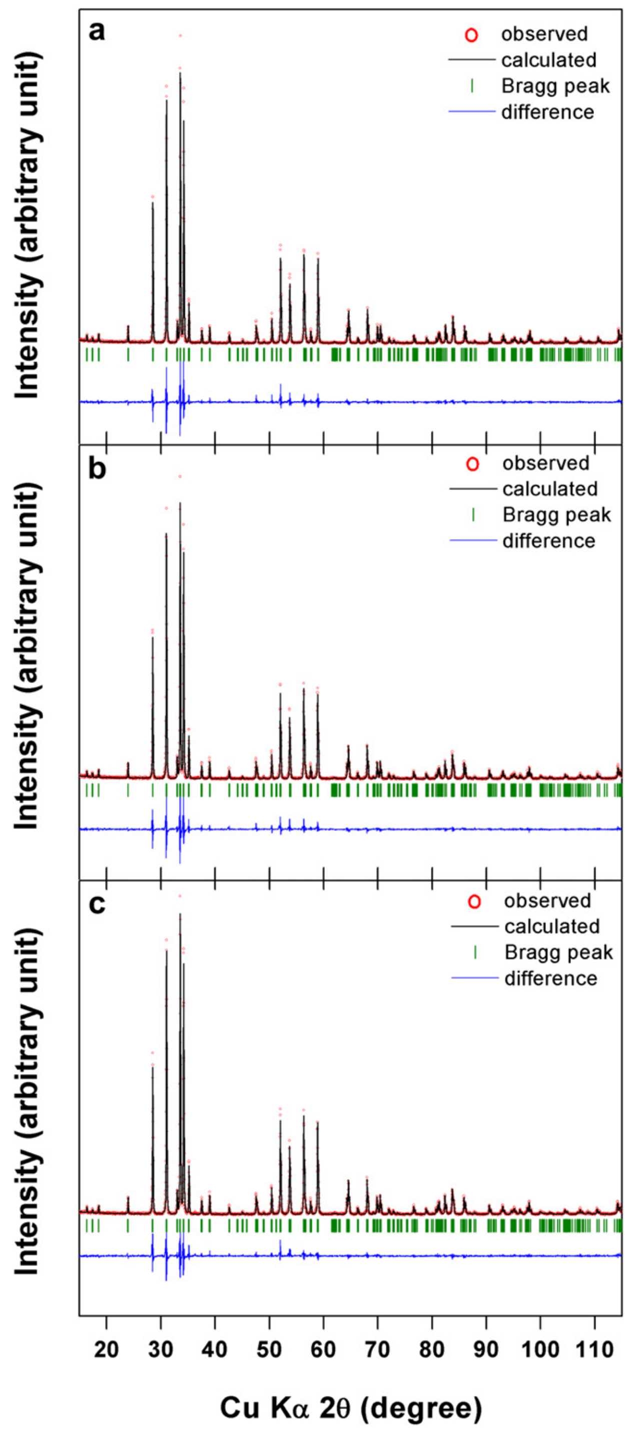

Fig. 1. Rietveld refinement of XRD patterns of the various $(Y_{0.5}In_{0.5})Ba(Co_{4-x}Zn_x)O_7$ samples: (a) $(Y_{0.5}In_{0.5})BaCo_3ZnO_7$ (x = 1), (b) $(Y_{0.5}In_{0.5})BaCo_{2.5}Zn_{1.5}O_7$ (x = 1.5), and (c) $(Y_{0.5}In_{0.5})BaCo_2Zn_2O_7$. The observed and calculated profiles, Bragg peak positions, and the difference between the observed and calculated profiles are shown.

ac-impedance spectroscopy (Solartron 1260 FRA). The GDC electrolyte disks were prepared by pelletizing and sintering required amounts of Gd_2O_3 and CeO_2 at 1600 °C for 10 h. All the composite cathode materials were mixed with an organic binder (Heraeus V006) to form a slurry and then applied onto both the sides of a dense GDC pellet (0.75 mm thickness) by screen printing. The $(Y_{0.5}In_{0.5})Ba(Co_{4-x}Zn_x)O_7$ + GDC cathodes were heated at 800–950 °C for 3 h.

Fuel cell performances of the $(Y_{0.5}In_{0.5})BaCo_3ZnO_7$ + GDC (50:50 wt.%) composite cathode was evaluated with the anode-supported single cells consisting of $(Y_{0.5}In_{0.5})BaCo_3ZnO_7$ + GDC composite|GDC|Ni + GDC (functional layer, dense)|Ni + GDC (porous). The anode-supported tri-layer half cell was prepared by a one-step dry pressing/co-firing process [31]. For the cathode, the $(Y_{0.5}In_{0.5})BaCo_3ZnO_7$ + GDC layers were applied to the thin electrolyte layer by heating at 850 °C for 3 h. Pt meshes and wires were attached to each electrode using Pt paste as current collector. During the single cell SOFC operation, humidified H_2 (~3% H_2O at 25 °C) and air were supplied, respectively, as fuel and oxidant at a rate of 100 $cm^3\ min^{-1}$. The area of each electrode was 0.5 cm^2. After the single cell SOFC tests, the microstructures of the cathodes were observed with a JEOL JSM-5610 scanning electron microscope (SEM).

3. Results and discussion

3.1. Crystal structure of $(Y_{0.5}In_{0.5})Ba(Co_{4-x}Zn_x)O_7$

The room temperature XRD patterns of the $(Y_{0.5}In_{0.5})Ba(Co_{4-x}Zn_x)O_7$ (x = 1, 1.5, and 2) oxides are shown in Fig. 1 along with the refinement carried out based on the space group of $P31c$ [20,23]. The room-temperature oxygen contents of the as-prepared powders were determined to be 7.04 by the iodometric titration method. The resulting structural parameters and the quality of refinements are listed in Table 1. The lattice parameters and unit cell volume of $(Y_{0.5}In_{0.5})Ba(Co_{4-x}Zn_x)O_7$ tend to increase with Zn content as observed before with the $YBaCo_{4-x}Zn_xO_7$ system [18]. The unit cell volume expansion with Zn content can be explained to be due to the larger ionic radii of Zn^{2+} compared to that of $Co^{2+/3+}$. The high temperature XRD data of the $(Y_{0.5}In_{0.5})BaCo_3ZnO_7$ sample was recorded in the temperature range of 20–800 °C in air. Each XRD pattern was refined using the Rietveld refinement method, and the variation of the lattice parameters with temperature is

Table 1
Room-temperature structural parameters of $Y_{1/2}In_{1/2}BaCo_{4-x}Zn_xO_7$ oxides determined by the Rietveld method based on the space group $P31c$. The atomic positions are Ba (2/3,1/3,1/2), Y/In (2/3,1/3,z), Co1/Zn1 (0,0,z), Co2/Zn2 (x,y,z), O1 (x,y,z), O2 (0,0,z), and O3 (x,y,z).

	x = 1.0	x = 1.5	x = 2.0
a (Å)	6.267	6.272	6.275
c (Å)	10.214	10.219	10.220
Vol (Å^3)	347.395	348.140	348.501
Y/In (z)	0.875	0.875	0.876
Co1/Zn1 (z)	0.434 (2)	0.433 (2)	0.433 (2)
Co2/Zn2 (x)	0.174 (3)	0.172 (5)	0.173 (4)
Co2/Zn2 (y)	0.833 (3)	0.830 (5)	0.831 (4)
Co2/Zn2 (z)	0.689 (1)	0.690 (1)	0.687 (1)
O1 (x)	0.510 (10)	0.509 (11)	0.507 (9)
O1 (y)	0.508 (10)	0.500 (11)	0.497 (9)
O1 (z)	0.749 (2)	0.753 (2)	0.745 (2)
O2 (z)	0.252 (3)	0.250 (2)	0.247 (3)
O3 (x)	0.135 (4)	0.132 (4)	0.128 (3)
O3 (y)	0.802 (4)	0.803 (4)	0.795 (3)
O3 (z)	0.501 (2)	0.496 (2)	0.497 (2)
R_p	11.64	11.46	10.18
R_{wp}	15.55	14.82	13.69
χ^2	2.006	2.013	1.981

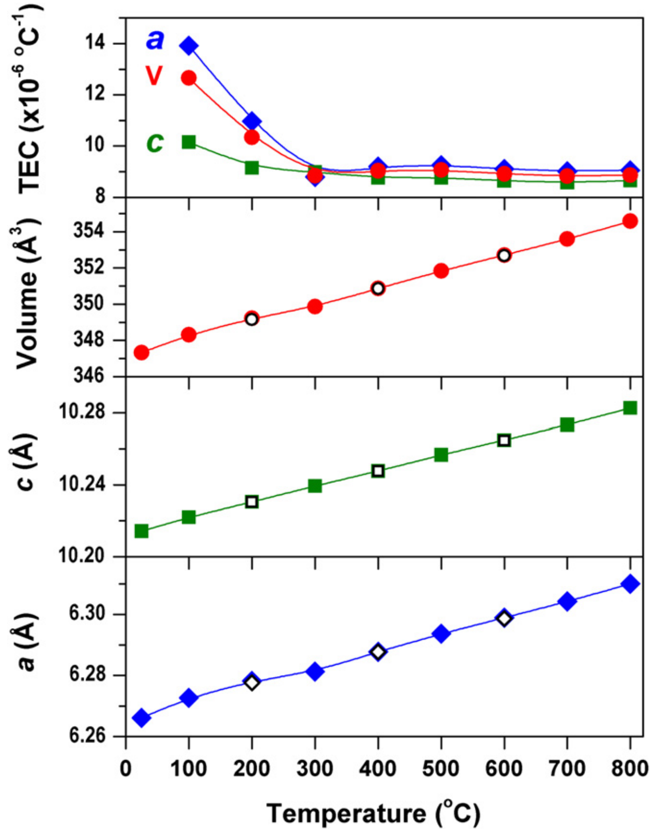

Fig. 2. Lattice parameters (a and c), unit cell volume (V), and TEC variations of the $(Y_{0.5}In_{0.5})BaCo_3ZnO_7$ (x = 1) samples measured during heating (closed symbols) and cooling (open symbols) by *in situ* XRD in air. Solid lines are a guide to the eye.

shown in Fig. 2. The lattice parameters and unit cell volume of the $(Y_{0.5}In_{0.5})BaCo_3ZnO_7$ increase with temperature, and the changes are quite reversible during heating (closed symbols) and cooling (open symbols). The TEC values were calculated based on the lattice parameter (a and c) and unit cell volume (V) values at various temperatures and are plotted in Fig. 2. Similar to the $InBaCo_{2.5}Zn_{1.5}O_7$ sample, the $(Y_{0.5}In_{0.5})BaCo_3ZnO_7$ sample exhibits anisotropic thermal expansion behavior with a larger expansion along the a axis [20]. The average TEC values are determined to be 8.6–9.1 × 10^{-6} °C^{-1} in the temperature range of 20–800 °C, which matches well with those of the standard electrolytes for intermediate temperature SOFC.

3.2. Oxygen content variation of $(Y_{0.5}In_{0.5})Ba(Co_{4-x}Zn_x)O_7$

The TGA results of the $(Y_{0.5}In_{0.5})BaCo_{4-x}Zn_xO_7$ samples were collected for two consecutive heating/cooling cycles in air. Fig. 3 shows the variation of the oxygen contents of $(Y_{0.5}In_{0.5})BaCo_{4-x}Zn_xO_{7+\delta}$ with temperature in air. To maximize the oxygen contents in the powder samples, there was a dwelling at 900 °C for 15 h during the first heating cycle. The first weight gain at $T < 300$ °C (on heating) is attributed to the oxygen absorption, characteristic of this class of materials where the excess oxygen partly transforms the original CoO_4 tetrahedra into CoO_6 octahedra that is accompanied by a drastic oxygen displacement and subsequent phase transition [32]. However, the sample loses the oxygen at $T > 300$ °C and shows a slight weight loss up to 900 °C. In our earlier study, $YBaCo_3ZnO_7$ showed a small weight gain at ~870 °C during the sintering process due to a filling up of the oxygen vacancies [18]. Similarly, the $(Y_{0.5}In_{0.5})BaCo_{4-x}Zn_xO_7$ powder samples also gain a small weight on dwelling at 900 °C in the first

Table 2
High-temperature phase stability, chemical analysis, TEC, and electrochemical data of the $(Y_{0.5}In_{0.5})BaCo_{4-x}Zn_xO_{7\pm\delta}$ oxides.

Chemical composition	Long-term stability test (100–120 h)[a]			Oxygen content $(7 \pm \delta)$[b]	Oxidation state of Co[c]	TEC × 10^6 ($^\circ C^{-1}$) 80–900 °C	Activation energy (eV)[d]	
	800 °C	700 °C	600 °C				Pristine	Composite
$YBaCo_3ZnO_{7\pm\delta}$	Good	Bad	Bad	7.07	2.38	9.5	0.82	0.94
$(Y_{0.5}In_{0.5})Ba(Co_3Zn)O_{7\pm\delta}$	Good	Good	Good	7.04	2.36	9.5	0.74	0.98
$(Y_{0.5}In_{0.5})Ba(Co_{2.5}Zn_{1.5})O_{7\pm\delta}$	Good	Good	Good	7.04	2.43	9.3	0.82	1.03
$(Y_{0.5}In_{0.5})Ba(Co_2Zn_2)O_{7\pm\delta}$	Good	Good	Good	7.04	2.54	9.7	0.95	1.06
$InBaCo_3ZnO_{7\pm\delta}$	Bad	Bad	Good	7.00	2.33	9.2	0.91	1.01

[a] The phase stability of $YBaCo_3ZnO_{7\pm\delta}$ was measured after dwelling at each temperature for 120 h, while the rest of the compositions were measured after 100 h.
[b,c] The oxygen content values and the oxidation state of Co were determined with as-synthesized samples at room temperature.
[d] The activation energy values were calculated from the Arrhenius plots of the polarization resistances (R_p) of the pristine cathodes and pristine + GDC (50:50 wt.%) composite cathodes in contact with GDC electrolyte in air.

cycle. Although all the as-synthesized samples ($x = 1$, 1.5, and 2) have the same initial oxygen contents of 7.04 (Table 2), they uptake different amounts of oxygen during annealing at 900 °C. As a result, at a given temperature, the oxygen content of $(Y_{0.5}In_{0.5})BaCo_{4-x}Zn_xO_{7+\delta}$ decreases with increasing Zn contents from $x = 1$ to 2. From TGA data, the $(Y_{0.5}In_{0.5})BaCo_{4-x}Zn_xO_{7+\delta}$ samples lose only a small weight (<0.3%) or amount of oxygen in the temperature range of 40–900 °C in air. Thus, the thermal expansion of the unit cell comes mainly from the normal expansion of the metal–oxygen bonds, and the chemical expansion due to the reduction of Co^{3+} ions to larger Co^{2+} ions is negligible.

3.3. Phase stability and thermal expansion behavior of $(Y_{0.5}In_{0.5})Ba(Co_{4-x}Zn_x)O_7$

The long-term phase stabilities of the $(Y_{0.5}In_{0.5})BaCo_{4-x}Zn_xO_7$ ($x = 1$, 1.5, and 2) were assessed by heating the pure powder samples at 600, 700, or 800 °C for specified hours, followed by quenching to room temperature. The In-free $YBaCo_3ZnO_7$ sample shows decomposition with peaks corresponding to $BaCoO_{3-\delta}$ after heating at 600 and 700 °C for 120 h, while it is stable at 800 °C for 120 h as seen in Fig. 4(a) [19]. In contrast, the Y-free $InBaCo_3ZnO_7$ sample shows decomposition after heating at 700 and 800 °C, respectively, for 100 and 12 h, while it is stable at 600 °C for 100 h as seen in Fig. 4(b) [20]. The decomposition product is found to be In_2O_3, $BaCoO_{3-z}$, and Co_3O_4 at 700 °C. However, it is interesting to note that the $(Y_{0.5}In_{0.5})BaCo_{4-x}Zn_xO_7$ ($x = 1$, 1.5, and 2) samples are stable at all the three temperatures (600, 700, and 800 °C) for 100 h as seen in Fig. 4(c)–(e). These findings suggest that employing a mixture of Y and In (50% each) promotes the phase stability and overcomes the phase-decomposition problems unlike that encountered with the $YBaCo_3ZnO_7$ and $InBaCo_3ZnO_7$ samples.

The thermal expansion behavior of the $(Y_{0.5}In_{0.5})BaCo_{4-x}Zn_xO_7$ ($x = 1$, 1.5, and 2) specimens were measured with the dilatometer in the temperature range of 80–900 °C in air with three consecutive heating/cooling curves, and the results are shown in Fig. 5. The corresponding TEC values are calculated to be 9.5 ($x = 1$), 9.3 ($x = 1.5$), and 9.7 ($x = 2$) × 10^{-6} $^\circ C^{-1}$ at 800 °C, which is slightly higher than that obtained with the high temperature XRD for the $x = 1.0$ sample (Fig. 2). All the specimens exhibit low TEC values that can provide good thermal expansion compatibility with the standard SOFC electrolyte materials such as yttria-stabilized zirconia (YSZ), GDC, and $La_{0.8}Sr_{0.2}Ga_{0.8}Mg_{0.2}O_{2.8}$ (LSGM) (10.0×10^{-6}–12.5×10^{-6} $^\circ C^{-1}$) [33,34].

3.4. Electrical conductivity and chemical stability of $(Y_{0.5}In_{0.5})Ba(Co_{4-x}Zn_x)O_7$

The total electrical conductivity variations of the $(Y_{0.5}In_{0.5})BaCo_{4-x}Zn_xO_7$ ($x = 1$, 1.5, and 2) specimens with temperature are shown in Fig. 6. The electrical conductivity increases with increasing temperature, indicating a thermally-activated polaron behavior [18]. The Arrhenius curves of Log σT vs. $1000/T$ are plotted in Fig. 6(b) from the temperature dependence of the electrical conductivity data. The energy barrier for the hole conduction activation energy (E_a) of the $(Y_{0.5}In_{0.5})BaCo_{4-x}Zn_xO_7$ ($x = 1$, 1.5, and 2) specimens are calculated to be 0.21 ($x = 1$), 0.24 ($x = 1.5$), and 0.28 eV ($x = 2$). At a given temperature, the $(Y_{0.5}In_{0.5})Ba(Co_{4-x}Zn_x)O_7$ samples exhibit a decrease in the electrical conductivity and an increase in the activation energy E_a with

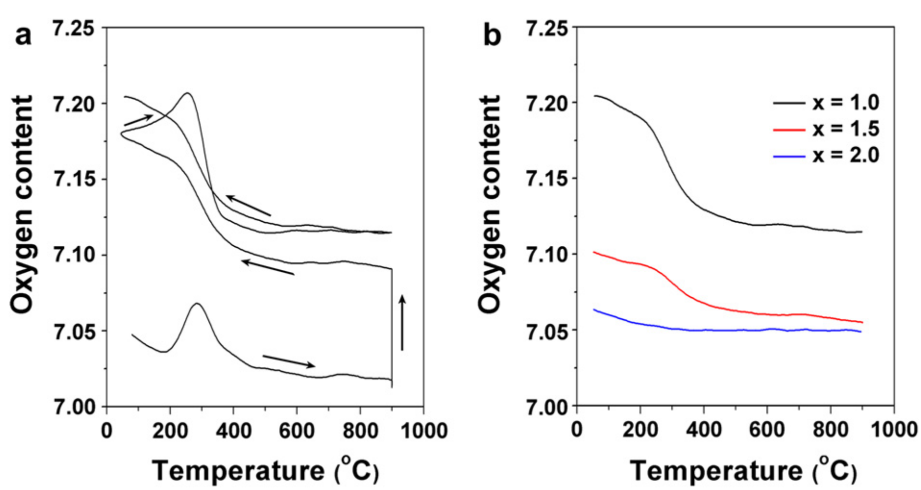

Fig. 3. TGA data of (a) $(Y_{0.5}In_{0.5})BaCo_3ZnO_7$ ($x = 1$) in the first and second heating and cooling and (b) $(Y_{0.5}In_{0.5})BaCo_{4-x}Zn_xO_7$ ($x = 1$, 1.5, and 2) recorded in the 2nd cooling with temperature in air.

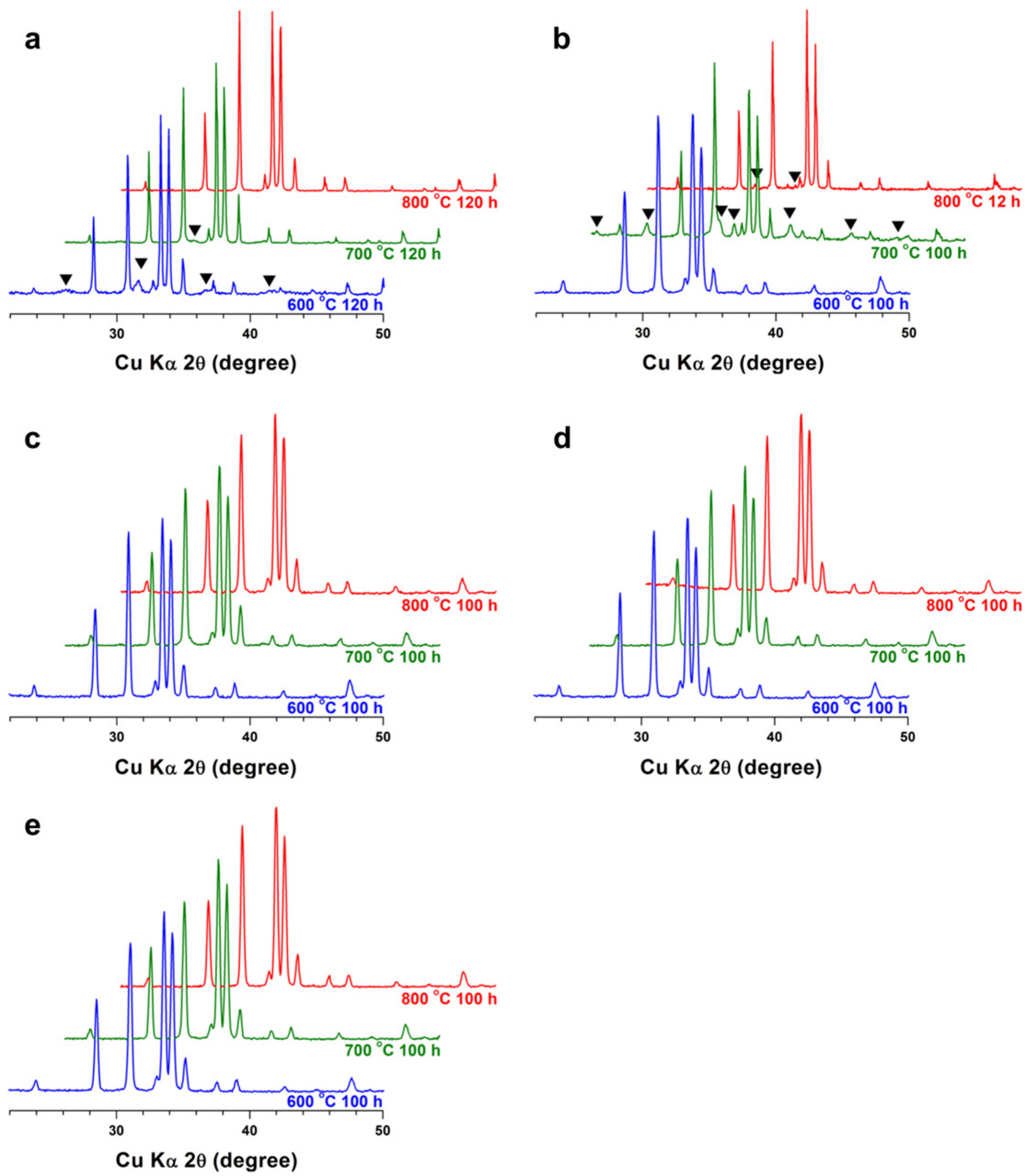

Fig. 4. XRD patterns of (a) $YBaCo_3ZnO_7$, (b) $InBaCo_3ZnO_7$, (c) $(Y_{0.5}In_{0.5})BaCo_3ZnO_7$ ($x = 1$), (d) $(Y_{0.5}In_{0.5})BaCo_{2.5}Zn_{1.5}O_7$ ($x = 1.5$), and (e) $(Y_{0.5}In_{0.5})BaCo_2Zn_2O_7$ ($x = 2$) after high temperature phase stability tests. The phase stability tests were performed at 600, 700, or 800 °C for 100–120 h, followed by quenching to room temperature. Reflections due to the formation of secondary phase are marked with ▼.

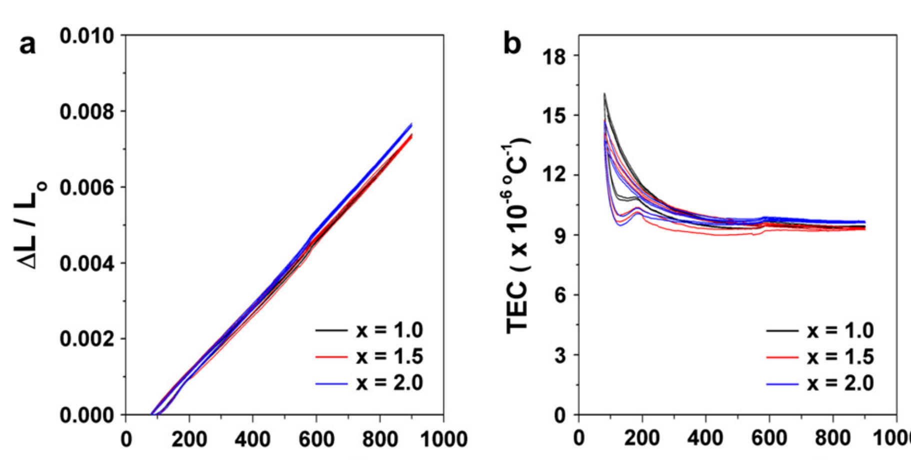

Fig. 5. Thermal expansion behaviors of the various $(Y_{0.5}In_{0.5})BaCo_{4-x}Zn_xO_7$ samples recorded at 80–900 °C in air: (a) $(Y_{0.5}In_{0.5})BaCo_3ZnO_7$, (b) $(Y_{0.5}In_{0.5})BaCo_{2.5}Zn_{1.5}O_7$, and (c) $(Y_{0.5}In_{0.5})BaCo_2Zn_2O_7$.

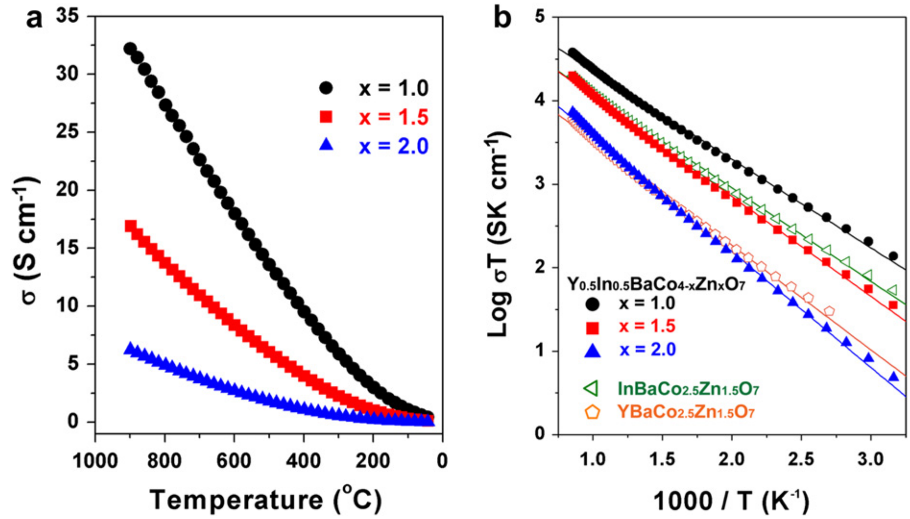

Fig. 6. (a) Variations of the electrical conductivity of $(Y_{0.5}In_{0.5})BaCo_{4-x}Zn_xO_7$ with $x = 1.0$, 1.5, 2.0, and (b) their Arrhenius plots with temperature in air in comparison to those of $InBaCo_{2.5}Zn_{1.5}O_7$ and $YBaCo_{2.5}Zn_{1.5}O_7$.

increasing Zn content from $x = 1$ to 2. This can be explained to be due to a perturbation of the electron hopping pathway by the Zn^{2+} (completely filled 3d orbital) substitution for $Co^{2+/3+}$ ions [18]. At a given Zn content of $x = 1.5$ and temperature (Fig. 6(b)), the $(Y_{0.5}In_{0.5})BaCo_{2.5}Zn_{1.5}O_7$ sample has higher conductivity than $YBaCo_{2.5}Zn_{1.5}O_7$, but lower than that of $InBaCo_{2.5}Zn_{1.5}O_7$.

The chemical stability between the $(Y_{0.5}In_{0.5})BaCo_{4-x}Zn_xO_7$ ($x = 1$, 1.5, and 2) samples and the GDC electrolyte was assessed by heating the mixtures at high temperatures. Fig. 7 shows the resulting XRD patterns with the two different phases marked. The $x = 1.0$, 1.5 (not shown), and 2 (not shown) samples are stable against GDC after heating the mixture at 800 and 1000 °C for 3 h. From our earlier study, a side reaction between $InBaCo_3ZnO_7$ and GDC has been reported after heating the mixture at 1000 °C for 3 h [20]. In contrast, the $YBaCo_{4-x}Zn_xO_7$ ($x = 1$, 1.5, and 2) samples are stable against GDC up to 1100 °C for 2 h. These results reveal that the presence of 50% Y in $(Y_{0.5}In_{0.5})Ba(Co_{4-x}Zn_x)O_7$ ($x = 1$, 1.5, and 2) improves the chemical stability significantly compared to the Y-free $InBaCo_{4-x}Zn_xO_7$ system. Thus the $(Y_{0.5}In_{0.5})BaCo_{4-x}Zn_xO_7$ ($x = 1$, 1.5, and 2) cathodes will not form any undesirable less-conductive side reaction products at the interface with GDC up to 1000 °C during the SOFC single-cell fabrication process.

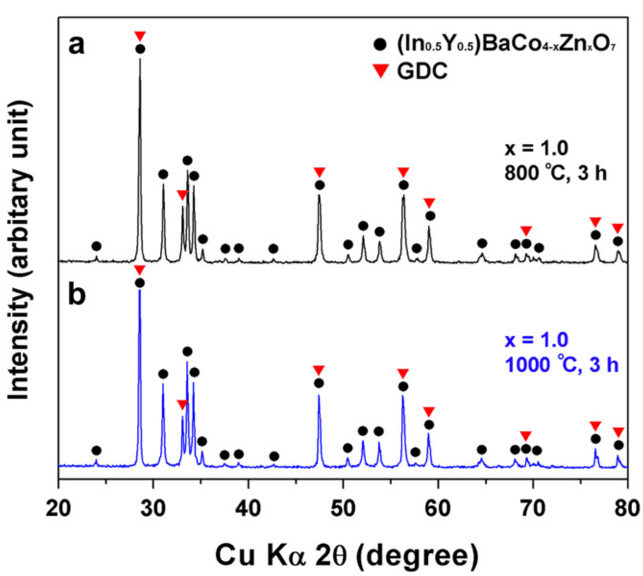

Fig. 7. Chemical stability of the $(Y_{0.5}In_{0.5})BaCo_3ZnO_7$ sample against GDC electrolyte. The data were collected after heating the 50:50 wt.% mixture of the $(Y_{0.5}In_{0.5})BaCo_3ZnO_7$ cathode and GDC powders at (a) 800 °C for 3 h and (b) 1000 °C for 3 h in air, followed by recording the XRD patterns at room temperature.

3.5. Cathode polarization resistance of $(Y_{0.5}In_{0.5})Ba(Co_{4-x}Zn_x)O_7$

Recently, $YBaCo_3ZnO_7$ was found to show good performance as a cathode at 500 °C < T < 700 °C, and optimum electrochemical performance was obtained by employing the $YBaCo_3ZnO_7$ + GDC (50:50 wt.%) composite as a cathode [18,21]. The composite cathodes are beneficial for providing extended triple-phase boundary (TPB) where the oxygen reduction reaction (ORR) occurs. It can also provide higher ionic conduction through the GDC portion in the composite cathode and better TEC compatibility with the GDC electrolyte [21].

Accordingly, we applied both the pristine $(Y_{0.5}In_{0.5})BaCo_{4-x}Zn_xO_7$ and the $(Y_{0.5}In_{0.5})BaCo_{4-x}Zn_xO_7$ + GDC (50:50 wt.%) composites ($x = 1$, 1.5, and 2) as cathodes in SOFC. The cathode polarization resistances (R_p) of the pristine and composite cathodes were measured with symmetrical cell configurations of cathode (composite cathode)|GDC|cathode (composite cathode). The ac-impedance spectra were fitted with an electrical circuit model consisting of $R_S(R_{GB}/CPE_{GB})(R_1/CPE_1)(R_2/CPE_2)$, where the R_S is from the Pt wire and the bulk resistance of the GDC electrolyte, (R_{GB}/CPE_{GB}) is from the grain boundary resistance, and the two consecutive (R_1/CPE_1) and (R_2/CPE_2) circuits are from the cathode [19–21]. The impedance at high and intermediate frequencies is associated with ion and electron transfer at the electrode|electrolyte, and current collector|electrode interfaces, while that at the low frequencies (R_2/CPE_2) is related to non-charge transfer, such as oxygen surface exchange and gas phase diffusion inside and outside of the electrode [35]. Fig. 8(a) shows the Arrhenius plots of the R_p of the pristine $(Y_{0.5}In_{0.5})BaCo_{4-x}Zn_xO_7$ ($x = 1$, 1.5, and 2) cathodes in comparison with the pristine $YBaCo_3ZnO_7$ and $InBaCo_3ZnO_7$ cathodes. For $x = 1$, the $YBaCo_3ZnO_7$ cathode exhibits more than one order lower R_p value compared to that of the $InBaCo_3ZnO_7$ cathode in the temperature range of 400 °C ≤ T ≤ 750 °C. The R_p values of the $(Y_{0.5}In_{0.5})BaCo_3ZnO_7$ cathode are in between them. At a given temperature, the pristine $(Y_{0.5}In_{0.5})BaCo_{4-x}Zn_xO_7$ cathodes show a trend of increasing R_p with increasing Zn content from $x = 1$ to 2 [19,20]. The E_a values are calculated to be 0.74, 0.82, and 0.95 eV, respectively, for $x = 1$, 1.5, and $x = 2$ in Table 2. Fig. 8(b) compares the R_p values of the $(Y_{0.5}In_{0.5})BaCo_3ZnO_7$ ($x = 1$) + GDC (50:50 wt.%) composite cathode with different cathode adhesion temperature (800–950 °C) in air.

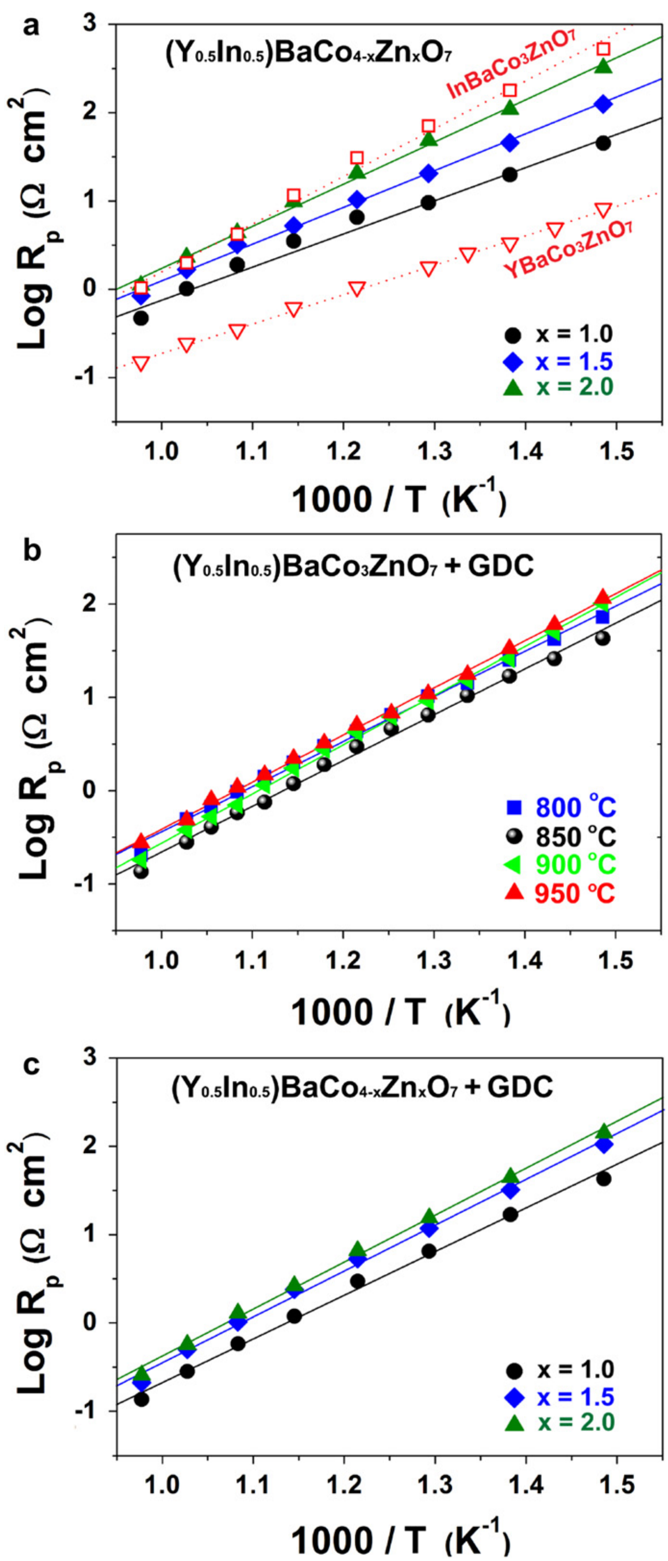

Fig. 8. Comparison of the R_p values of (a) pristine $(Y_{0.5}In_{0.5})BaCo_{4-x}Zn_xO_7$ cathodes attached at 850 °C for 3 h, (b) $(Y_{0.5}In_{0.5})BaCo_3ZnO_7$ + GDC (50:50 wt.%) composite cathodes attached at different temperatures for 3 h, and (c) $(Y_{0.5}In_{0.5})BaCo_{4-x}Zn_xO_7$ + GDC composite cathodes attached at 850 °C for 3 h.

Although all the $x = 1$ composite cathodes show lower R_p compared to the pristine $(Y_{0.5}In_{0.5})BaCo_3ZnO_7$ cathode (Fig. 8(a)) regardless of temperatures, the optimum adhesion temperature was determined to be 850 °C for 3 h with the lowest R_p values. Again, the $(Y_{0.5}In_{0.5})BaCo_{4-x}Zn_xO_7$ ($x = 1$, 1.5, 2) + GDC composite cathodes exhibit increasing R_p with Zn content x at a given temperature in Fig. 8(c). The E_a values of the composite cathodes are calculated to be 0.98, 1.03, and 1.06 eV, respectively, for $x = 1$, 1.5, and $x = 2$ in Table 2. The composite cathodes exhibit higher E_a than the pristine cathodes since the GDC in the composite has high E_a (~1.0 eV) for the ionic conductivity [24]. From the results, the lowest R_p value could be obtained by employing the $(Y_{0.5}In_{0.5})BaCo_3ZnO_7$ + GDC (50:50 wt.%) composite cathode attached onto the GDC electrolyte at 850 °C for 3 h.

3.6. Cathode performance of $(Y_{0.5}In_{0.5})BaCo_3ZnO_7$ + GDC composite cathode

The fuel cell performance of the $(Y_{0.5}In_{0.5})BaCo_3ZnO_7$ + GDC (50:50 wt.%) composite cathode was evaluated by attaching at 850 °C for 3 h onto the top of anode-supported single cells with GDC thin-film electrolyte (~20 μm thickness). In Fig. 9, the open-circuit voltage (OCV) of the single cell is ~0.8 V at 600 °C and decreases with increasing temperature that agrees well with the literature [36,37]. These OCV values are significantly lower than the theoretical values obtained from Nernst equation due to the reduction of the Ce^{4+} ions in GDC and a subsequent increase in electronic conduction with increasing temperature. The I–V curves were measured at 700, 675, 650 °C, and the corresponding power density values of the single cell were found to be 521, 375, and 252 mW cm^{-2}. The $(Y_{0.5}In_{0.5})BaCo_3ZnO_7$ + GDC composite cathode showed enhanced electrochemical performances compared to our earlier reports based on the trigonal $(Y_{0.5}Ca_{0.5})BaCo_{2.5}Zn_{1.5}O_7$ + GDC composite cathode (450 mW cm^{-2} at 700 °C) and the perovskite-related $Nd(Sr_{2.5}Ca_{0.5})(Fe_{1.5}Co_{1.5})O_{10}$ composite cathode (357 mW cm^{-2} at 700 °C) with the same single cell configuration [19,38,39]. However, the power density is still low at 600 °C, and further optimization of the GDC thin-film electrolyte could help to improve the performance comparable to that of Co-based perovskite oxides, based on the polarization resistance studies in our earlier reports [18,19].

Fig. 10(a) represents the microstructure of the cross sectional SEM image of the anode-supported single cell after the fuel cell performance test. The bottom of the micrograph indicates the porous Ni + GDC anode layer, while the functional layer placed between the porous anode and the GDC electrolyte shows less porous layer with

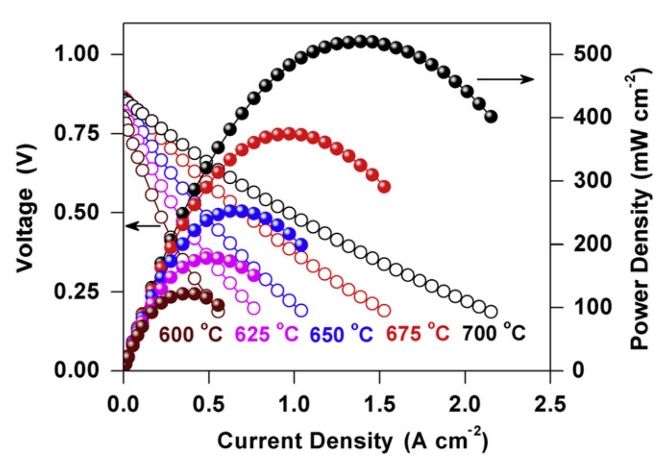

Fig. 9. Single cell SOFC performances of the $(Y_{0.5}In_{0.5})BaCo_3ZnO_7$ + GDC (50:50 wt.%) composite cathodes at 700 °C (521 mW cm^{-2}), 675 °C (375 mW cm^{-2}), 650 °C (252 mW cm^{-2}), 625 °C (178 mW cm^{-2}), and 600 °C (122 mW cm^{-2}).

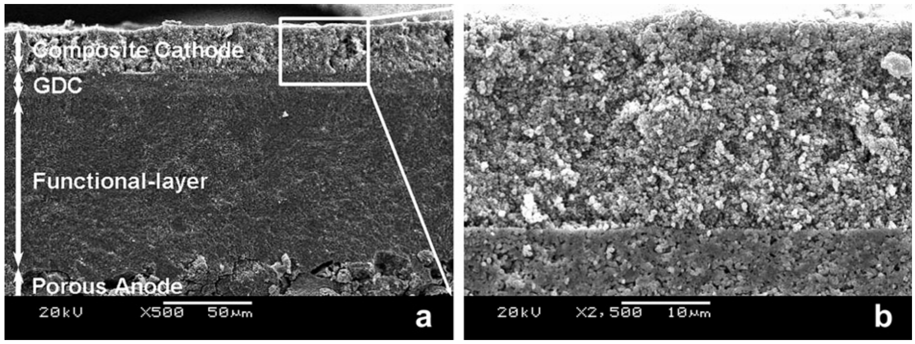

Fig. 10. Microstructure of the (a) anode-supported single cell cross sections consisting of $(Y_{0.5}In_{0.5})BaCo_3ZnO_7$ + GDC composite cathode|GDC|functional anode layer|porous anode and (b) expanded interface section of the $(Y_{0.5}In_{0.5})BaCo_3ZnO_7$ + GDC composite cathode|GDC electrolyte.

a thickness of ~120 μm. Around 20 μm thick dense GDC electrolyte with closed pores provides good separation between the anode and cathode layer. The porous microstructure of the $(Y_{0.5}In_{0.5})BaCo_3ZnO_7$ + GDC composite cathode is shown in Fig. 10(b).

Among the various compositions investigated in the $RBaCo_{4-x}Zn_xO_7$ family, the R = $Y_{0.5}In_{0.5}$ (x = 1, 1.5, and 2) samples demonstrate an important advantage of phase stability at the operating temperatures of SOFC (600–800 °C) in Fig. 4, while maintaining its benefit of the low TEC values (Figs. 2and 5). Furthermore, the $Y_{0.5}In_{0.5}BaCo_3ZnO_7$ composition overcomes the chemical instability problem against GDC electrolyte that was observed with the $InBaCo_3ZnO_7$ composition after heating at 1000 °C for 3 h [30]. On employing the $(Y_{0.5}In_{0.5})BaCo_3ZnO_7$ + GDC composite as a cathode, lower R_p values (Fig. 8(b) and (c)) and promising fuel cell performances could be achieved.

4. Conclusions

The properties of the $(Y_{0.5}In_{0.5})BaCo_{4-x}Zn_xO_7$ system with R = $Y_{0.5}In_{0.5}$ have been studied in comparison to the end members $YBaCo_{4-x}Zn_xO_7$ and $InBaCo_{4-x}Zn_xO_7$. The $YBaCo_3ZnO_7$ sample decomposes at 600 and 700 °C over 120 h, while the $InBaCo_3ZnO_7$ sample decomposes at 700 and 800 °C over 100 h. Interestingly, the presence of 50% Y and 50% In in $(Y_{0.5}In_{0.5})Ba(Co_3Zn)O_7$ eliminates these instability problems, providing good long-term phase stability at high temperatures (600, 700, and 800 °C for 100 h). The improved phase stability of the solid solution with 50% Y and 50% In allows the incorporation of higher Co contents (x = 1) without encountering phase decomposition compared to the In- or Y-free samples. The higher Co content is beneficial to realize good electrochemical performance due to enhanced electrical conductivity, while keeping the TEC low and maintaining good long-term phase stability at 600–800 °C for 100 h. The $(Y_{0.5}In_{0.5})Ba(Co_3Zn)O_7$ + GDC (50:50 wt.%) composite cathode exhibits SOFC performance superior to other composite cathodes such as trigonal $(Y_{0.5}Ca_{0.5})BaCo_{2.5}Zn_{1.5}O_7$ and perovskite-related $Nd(Sr_{2.5}Ca_{0.5})(Fe_{1.5}Co_{1.5})O_{10}$ at 700 °C with the same single cell configuration. Our future work will focus on evaluating the performance of $(Y_{0.5}In_{0.5})Ba(Co,Zn)_4O_7$ with YSZ and LSGM electrolytes and their long-term stability during thermal cycling in the fuel cell.

Acknowledgments

Financial support for the work carried at the University of Texas at Austin by the Welch Foundation grant F-1254 and National Science Foundation MIRT grant DMR-1122603 is gratefully acknowledged by Young Nam Kim and Arumugam Manthiram. Research carried out at Oak Ridge National Laboratory (ORNL) was supported by the Laboratory Directed Research and Development (LDRD) Program of ORNL and Jung-Hyun Kim acknowledges the support of ORISE postdoctoral fellowship. Ashfia Huq acknowledges Spallation Neutron Source for financial support which is supported by the Division of Scientific User Facilities, Office of Basic Energy Sciences, U.S. Department of Energy.

References

[1] D.J.L. Brett, A. Atkinson, N.P. Brandon, S.J. Skinner, Chem. Soc. Rev. 37 (2008) 1568.
[2] N.Q. Minh, T. Takahashi, Science and Technology of Ceramic Fuel Cells, Elsevier, Amsterdam, 1995.
[3] H.J.M. Bouwmeestere, A.J. Burggraaf, The CRC Handbook of Solid State Electrochemistry, CRC Press, New York, 1997.
[4] J.-M. Bae, B.C.H. Steele, Solid State Ionics 106 (1998) 247.
[5] E.P. Murray, M.J. Sever, S.A. Barnett, Solid State Ionics 148 (2002) 27.
[6] J.-H. Kim, A. Manthiram, J. Electrochem. Soc. 155 (2008) B385.
[7] A. Tarancon, S.J. Skinner, R.J. Chater, F. Hernandez-Ramirez, J.A. Kilner, J. Mater. Chem. 17 (2007) 3175.
[8] Y.N. Kim, J.-H. Kim, A. Manthiram, J. Power Sources 195 (2010) 6411.
[9] Y.N. Kim, A. Manthiram, J. Electrochem. Soc. 158 (2011) B276.
[10] A. Manthiram, F. Prado, T. Armstrong, Solid State Ionics 152 (2002) 647.
[11] F. Prado, A. Manthiram, J. Solid State Chem. 158 (2001) 307.
[12] K.T. Lee, D.M. Bierschenk, A. Manthiram, J. Electrochem. Soc. 153 (2006) A1255.
[13] T. Armstrong, F. Prado, A. Manthiram, Solid State Ionics 140 (2001) 89.
[14] C. Torres-Garibay, D. Kovar, J. Power Sources 192 (2009) 396.
[15] M. Mori, Y. Hiei, N.M. Sammes, G.A. Tompsett, J. Electrochem. Soc. 147 (2000) 1295.
[16] M.T. Colomer, B.C.H. Steele, J.A. Kilner, Solid State Ionics 147 (2002) 41.
[17] A.N. Petrov, O.F. Kononchuk, A.V. Andreev, V.A. Cherepanov, P. Kofstad, Solid State Ionics 80 (1995) 189.
[18] J.-H. Kim, A. Manthiram, Chem. Mater. 22 (2010) 822.
[19] Y.N. Kim, J.-H. Kim, A. Manthiram, Int. J. Hydrogen Energy 36 (2011) 15295.
[20] J.-H. Kim, Y.N. Kim, Z. Bi, A. Manthiram, M.P. Paranthaman, A. Huq, Electrochim. Acta 56 (2011) 5740.
[21] J.-H. Kim, Y.N. Kim, S.M. Cho, H. Wang, A. Manthiram, Electrochim. Acta 55 (2010) 5312.
[22] V.B. Vert, J.M. Serra, J.L. Jordá, Electrochem. Commun. 12 (2010) 278.
[23] A. Huq, J.F. Mitchell, H. Zheng, L.C. Chapon, P.G. Radaelli, K.S. Knight, P.W. Stephens, J. Solid State Chem. 179 (2006) 1136.
[24] M. Valldor, Solid State Sci. 6 (2004) 251.
[25] A. Maignan, V. Caignaert, D. Pelloquin, S. Hebert, V. Pralong, J. Hejtmanek, D. Khomskii, Phys. Rev. B 74 (2006) 1651101.
[26] H.S. Hao, J.H. Cui, C.Q. Chen, L.J. Pan, J. Hu, X. Hu, Solid State Ionics 177 (2006) 631.
[27] B.H. Toby, J. Appl. Crystallogr. 34 (2001) 210.
[28] A. Manthiram, J.S. Swinnea, Z.T. Sui, H. Steinfink, J.B. Goodenough, J. Am. Chem. Soc. 109 (1987) 6667.
[29] L.J. van der Pauw, Philips Res. Rep. 13 (1958) 1.
[30] I. Riess, J. Appl. Phys. 71 (1992) 4079.
[31] B. Lin, J. Chen, Y. Ling, X. Zhang, Y. Jiang, L. Zhao, X. Liu, G. Meng, J. Power Sources 195 (2010) 1624.
[32] O. Chmaissem, H. Zheng, A. Huq, P.W. Stephens, J.F. Mitchell, J. Solid State Chem. 181 (2008) 664.
[33] H. Ullmann, N. Trofimenco, F. Tietz, D. Stöver, A. Ahmad-Khanlou, Solid State Ionics 138 (2000) 79.
[34] V.V. Kharton, F.M.B. Marques, A. Atkinson, Solid State Ionics 174 (2004) 135.
[35] S.B. Adler, X.Y. Chen, J.R. Wilson, J. Catal. 245 (2007) 91.
[36] M. Godickemeier, K. Sasaki, L.J. Gauckler, I. Riess, J. Electrochem. Soc. 144 (1997) 1635.
[37] M. Godickemeier, L.J. Gauckler, J. Electrochem. Soc. 145 (1998) 414.
[38] Y.N. Kim, A. Manthiram, J. Electrochem. Soc. 158 (2011) B1206.
[39] J.-H. Kim, K.-T. Lee, Y.N. Kim, A. Manthiram, J. Mater. Chem. 21 (2011) 2482.